

HIGGS-PAIR PRODUCTION VIA GLUON FUSION: TOP-YUKAWA- AND LIGHT-QUARK-INDUCED ELECTROWEAK CORRECTIONS

A. BHATTACHARYA¹, F. CAMPANARIO¹, S. CARLOTTI², J. CHANG^{3,4}, J. MAZZITELLI³,
M. MÜHLLEITNER², J. RONCA⁵, AND M. SPIRA³

¹ *Theory Division, IFIC, University of Valencia-CSIC, E-46980 Paterna, Valencia, Spain*

² *Institute for Theoretical Physics, KIT, D-76128 Karlsruhe, Germany*

³ *PSI Center for Neutron and Muon Sciences, CH-5232 Villigen PSI, Switzerland*

⁴ *Institute for Theoretical Physics, ETH Zürich, CH-8093 Zürich, Switzerland*

⁵ *Dipartimento di Fisica e Astronomia, Università degli Studi di Padova, and INFN, Sezione di Padova, Via Marzolo 8, I-35131 Padova, Italy*

Abstract

Gluon fusion, $gg \rightarrow HH$, is the dominant Higgs-pair production process at the Large Hadron Collider (LHC) and provides the first direct access to the trilinear Higgs self-interaction. The process is loop-induced, with the main contribution emerging from top-quark loops within the Standard Model. In the past, the QCD corrections have been calculated and found to increase the cross section significantly. With the anticipated accuracies achievable at the high-luminosity LHC (HL-LHC), the theoretical uncertainties will be of increased relevance to compete with the experimental precision at the level of less than 30%. In this work, we take the next steps towards the determination of the complete electroweak corrections at next-to-leading order by calculating the full top-Yukawa and light-quark induced corrections. These corrections modify the cross section moderately in the kinematical regimes of interest.

1 Introduction

After the discovery of the Higgs boson in 2012 [1], increasingly precise measurements have been made to determine its properties [2]. Early experiments confirmed that its spin and CP were consistent with the spinless and CP-even nature of the Standard Model (SM) Higgs boson. Subsequent measurements of the boson's couplings to the top and bottom quarks, the τ lepton, and the electroweak gauge bosons, W and Z , further supported the SM-like nature by showing agreement with the SM predictions within their respective experimental uncertainties. Moreover, the loop-induced couplings to photons and gluons have been determined, and recently, evidence for Higgs couplings to second-generation muons and to $Z\gamma$ has been found [3]. So far, no deviations from the properties of the SM Higgs boson have been observed. In addition to probing the Higgs boson couplings to muons and charm quarks, one of the major goals of the HL-LHC is the measurement of the trilinear Higgs self-coupling λ_{HHH} , as the first step towards the experimental reconstruction of the scalar Higgs potential [4].

The Higgs sector of the SM consists of a scalar isospin doublet containing three would-be Goldstone bosons and one physical Higgs field [5]. The latter acquires a finite vacuum expectation value resulting in a non-trivial realization of the electroweak gauge symmetry. The

fluctuations of the scalar Higgs field around this vacuum expectation value describe the Higgs boson as part of the physical states of the SM. The Higgs boson allows the gauge symmetry to be unbroken, so that the electroweak interactions are weak up to high-energy scales [6] and crucially, renormalizable [7]. At the LHC, the SM Higgs boson is dominantly produced in the loop-induced gluon fusion process $gg \rightarrow H$, while all the other production modes, vector-boson fusion $qq \rightarrow qqH$, Higgs-strahlung $q\bar{q} \rightarrow W/Z + H$ and bremsstrahlung off top quarks $gg/q\bar{q} \rightarrow t\bar{t}H$, are suppressed by at least one order of magnitude (see, e.g. [8]).

The trilinear Higgs self-coupling will first become directly accessible in Higgs-boson pair production [9]. The dominant Higgs-boson pair production channel is gluon fusion $gg \rightarrow HH$, while the other processes, vector-boson fusion $qq \rightarrow qqHH$, double Higgs-strahlung $q\bar{q} \rightarrow HH + W/Z$ and associated production with a $t\bar{t}$ pair $gg, q\bar{q} \rightarrow t\bar{t}H$, are suppressed by an order of magnitude or more. The pair production processes are suppressed by three orders of magnitude compared to their single Higgs counterparts. In this work, we focus on the dominant gluon fusion process. The leading order (LO) cross section was calculated a long time ago [10] and the QCD corrections were calculated at next-to-leading order (NLO) [11], next-to-NLO (NNLO) [12] and next-to-NNLO (N^3LO) [13] in the heavy-top limit (HTL). These contributions increase the cross section by more than a factor of two. More recently, the full NLO QCD corrections, including the full top-quark mass dependence, have become available. These corrections reduce the total cross section by approximately 15% relative to the Born-improved HTL, although their impact is more pronounced in differential distributions [14–16]. These calculations were performed by applying two different methods of numerical integration. This has been supported by suitable expansion methods in the low- and high-energy regimes, as well as covering the full kinematical range [17, 18]. The complete NLO results were combined with the NNLO corrections in the HTL with the full mass dependence included in the double-real corrections [19]. In addition, soft-gluon resummation effects have been studied up to next-to-next-to-next-to-leading logarithmic order (N^3LL) [20]. The grids of the full numerical calculation were implemented in **POWHEG-BOX** and **aMC@NLO** [21] and, recently, in the Geneva generator [22]. In addition, the expansion approach [18] was linked to **POWHEG-BOX** so that it yields reliable results at the per-cent-level accuracy in the full kinematical range. However, the theoretical uncertainties were found to be dominated by the scale and scheme dependence of the virtual top mass and amount to a maximum of 25% for the total cross section. These uncertainties are larger for kinematical distributions [15, 16, 18]. Dedicated efforts are required to reduce them to at-most the level of 10%. The full NNLO QCD corrections are partly known meanwhile [23], but are not yet complete. Another approach has analyzed the leading logarithmic structure of the cross section by using SCET methods at high energies [24]. A reduction of the scale and scheme dependence at high energy, however, requires the analysis to be extended to the subleading logarithmic level and to the low-energy regime close to the production threshold and the virtual $t\bar{t}$ -threshold, which is beyond the work of Ref. [24].

The next step in reducing the theoretical uncertainties is to calculate the NLO electroweak corrections. The first work in this direction has determined the top-Yukawa-induced corrections in the HTL for the effective Higgs couplings to gluons, while the trilinear Higgs-vertex corrections have been included with full mass dependence [26]. This analysis has pointed out that the use of a radiatively corrected effective trilinear Higgs coupling is disfavored upon com-

parison with the results using the LO-like coupling. The first complete electroweak corrections to Higgs boson pair production have been obtained in Ref. [27]. These corrections reach the -10% level at large invariant Higgs-pair masses M_{HH} , while more pronounced effects appear near the production threshold $M_{HH} \gtrsim 2M_H$ due to the large destructive interference effects of the LO matrix element, rendering this regime as sub-leading for the physical observable. Although the results of Ref. [27] are technically comprehensive, a decomposition into individually identifiable contributions is not yet known. Consequently, further analytic insight into the underlying mechanisms remains valuable for understanding the origin and kinematic features of the electroweak corrections. Recently, a complete numerical calculation of the top-Yukawa- and Higgs self-interaction-induced corrections has been presented, where only Higgs-exchange diagrams have been taken into account [28]. For large values of M_{HH} , analytical high-energy expansions exist, which confirm the small size of the top-Yukawa-induced corrections [29]. The contribution of light-quark loops has also been derived and found to be small [30].

This work presents the first dedicated numerical evaluation of the full top-Yukawa-induced corrections involving Higgs and Goldstone boson exchange diagrams, as well as the light-quark loop contributions. These results provide a physically transparent decomposition of the electroweak effects, complementing existing calculations by isolating and quantifying the contributions of individual diagram classes. In Section 2, we review the LO results and define our notation. Section 3 describes our method to perform the numerical integration and renormalization, while in Section 4 we present our results. In Section 5, we conclude this work by summarizing our findings.

2 Higgs-boson pair production via gluon fusion

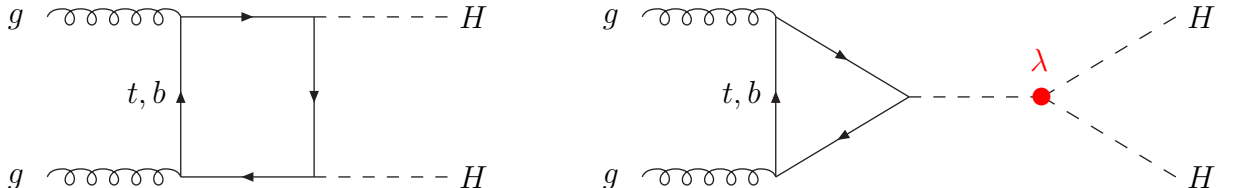


Figure 1: *Typical diagrams of Higgs-boson pair production via gluon fusion at LO. The contribution of the trilinear Higgs coupling is marked in red.*

At LO, Higgs pair production is generated primarily by top-quark loops, with minor contributions from bottom-quark loops. The contributing diagrams are shown in Fig. 1 and are grouped into two classes, box and triangle diagrams, where the latter contains an s -channel Higgs propagator and the trilinear Higgs coupling $\lambda = \lambda_{HHH}$. At this order, the total and differential

production cross sections with respect to the invariant Higgs-pair mass are given by

$$\begin{aligned}\sigma_{\text{LO}} &= \int_{\tau_0}^1 d\tau \frac{d\mathcal{L}^{gg}}{d\tau} \hat{\sigma}_{\text{LO}}(Q^2 = \tau s) \\ \frac{d\sigma_{\text{LO}}}{dQ^2} &= \frac{d\mathcal{L}^{gg}}{d\tau} \frac{\hat{\sigma}_{\text{LO}}(Q^2)}{s} \Big|_{\tau = \frac{Q^2}{s}},\end{aligned}\quad (1)$$

where \mathcal{L}^{gg} denotes the gluonic parton luminosity involving the gluon densities $g(x, \mu_F)$,

$$\frac{d\mathcal{L}^{gg}}{d\tau} = \int_{\tau}^1 \frac{dx}{x} g(x, \mu_F) g\left(\frac{\tau}{x}, \mu_F\right) \quad (2)$$

at the factorization scale μ_F , and the integration boundary is given by $\tau_0 = 4M_H^2/s$, where s denotes the hadronic center-of-mass (c.m.) energy squared and M_H the Higgs mass. The scale $Q^2 = M_{HH}^2$ is defined in terms of the invariant mass M_{HH} of the Higgs pair. The partonic cross section at LO can be cast into the form

$$\hat{\sigma}_{\text{LO}} = \frac{G_F^2 \alpha_s^2(\mu_R)}{512(2\pi)^3} \int_{\hat{t}_-}^{\hat{t}_+} d\hat{t} \left[|C_{\Delta} F_{\Delta} + F_{\square}|^2 + |G_{\square}|^2 \right], \quad (3)$$

where the integration boundaries are given by

$$\hat{t}_{\pm} = -\frac{1}{2} \left[Q^2 - 2M_H^2 \mp Q^2 \sqrt{1 - 4 \frac{M_H^2}{Q^2}} \right], \quad (4)$$

and the symmetry factor $1/2$ for the identical Higgs bosons in the final state is included. The coefficient $C_{\Delta} = v \lambda_{HHH} / (Q^2 - M_H^2)$ contains the LO trilinear Higgs coupling

$$\lambda_{HHH} = 3 \frac{M_H^2}{v}, \quad (5)$$

that is related to the Higgs mass and the vacuum expectation value (vev) v , where the vev is connected to the Fermi constant $G_F = 1/(\sqrt{2}v^2)$. The factor $\alpha_s(\mu_R)$ denotes the strong coupling at the renormalization scale μ_R . The form factors F_{Δ} of the LO triangle diagrams and F_{\square}, G_{\square} of the LO box diagrams can be found in Refs. [10]. In the HTL, they approach simple expressions: $F_{\Delta} \rightarrow 2/3$, $F_{\square} \rightarrow -2/3$ and $G_{\square} \rightarrow 0$.

3 Electroweak corrections

In this section, we discuss the top-Yukawa and light-quark induced electroweak corrections, with the latter neglecting the virtual quark masses. Since the electroweak corrections do not involve real corrections, their total sum is infrared and collinear finite. Therefore, the NLO corrections can be accommodated by a shift of the corresponding LO form factors

$$F_{\Delta} \rightarrow F_{\Delta} (1 + \Delta_{\Delta}), \quad F_{\square} \rightarrow F_{\square} (1 + \Delta_{\square}), \quad G_{\square} \rightarrow G_{\square} (1 + \Delta_G). \quad (6)$$

From this, one can expand Eq. (3) in the electroweak couplings. At NLO, the result reads

$$\frac{d\sigma_{NLO}}{dQ^2} = \frac{d\sigma_{LO}}{dQ^2} (1 + \delta) \quad (7)$$

with

$$\delta = 2\Re e \frac{\int_{\hat{t}_-}^{\hat{t}_+} dt \left[(C_\Delta F_\Delta + F_\square)^* (C_\Delta F_\Delta \Delta_\Delta + F_\square \Delta_\square) + |G_\square|^2 \Delta_G \right]}{\int_{\hat{t}_-}^{\hat{t}_+} dt \left[|C_\Delta F_\Delta + F_\square|^2 + |G_\square|^2 \right]}, \quad (8)$$

There are two tensor structures that contribute to the matrix element, corresponding to the total angular-momentum states with $S_z = 0$ and 2 ,

$$\mathcal{M}[g^a(q_1)g^b(q_2) \rightarrow H(p_1)H(p_2)] = -i \delta_{ab} \frac{G_F \alpha_s(\mu_R) Q^2}{2\sqrt{2}\pi} \mathcal{A}^{\mu\nu} \epsilon_{1\mu} \epsilon_{2\nu},$$

$$\begin{aligned} \text{where} \quad \mathcal{A}^{\mu\nu} &= F_1 T_1^{\mu\nu} + F_2 T_2^{\mu\nu}, \\ F_1 &= C_\Delta F_\Delta + F_\square, & F_2 &= G_\square, \\ \text{and} \quad T_1^{\mu\nu} &= g^{\mu\nu} - \frac{q_1^\nu q_2^\mu}{(q_1 q_2)}, \\ T_2^{\mu\nu} &= g^{\mu\nu} + \frac{M_H^2 q_1^\nu q_2^\mu}{p_T^2 (q_1 q_2)} - 2 \frac{(q_2 p_1) q_1^\nu p_1^\mu}{p_T^2 (q_1 q_2)} - 2 \frac{(q_1 p_1) p_1^\nu q_2^\mu}{p_T^2 (q_1 q_2)} + 2 \frac{p_1^\nu p_1^\mu}{p_T^2}, \\ \text{with} \quad p_T^2 &= 2 \frac{(q_1 p_1)(q_2 p_1)}{(q_1 q_2)} - M_H^2, \end{aligned} \quad (9)$$

where p_T is the transverse momentum of each of the final-state Higgs bosons. Working in $n = 4 - 2\epsilon$ dimensions, the following projectors can be constructed on the two form factors,

$$P_1^{\mu\nu} = \frac{(1 - \epsilon) T_1^{\mu\nu} + \epsilon T_2^{\mu\nu}}{2(1 - 2\epsilon)}, \quad P_2^{\mu\nu} = \frac{\epsilon T_1^{\mu\nu} + (1 - \epsilon) T_2^{\mu\nu}}{2(1 - 2\epsilon)}, \quad (10)$$

such that

$$P_1^{\mu\nu} \mathcal{A}_{\mu\nu} = F_1, \quad P_2^{\mu\nu} \mathcal{A}_{\mu\nu} = F_2. \quad (11)$$

Using these projectors, the explicit results of the two form factors $F_{1,2}$ can be obtained in a straightforward manner at LO and NLO.

3.1 Top–Yukawa-induced electroweak corrections

In order to define the top–Yukawa induced electroweak corrections consistently, we work in the gaugeless limit for these contributions [25]. This is defined by switching off electroweak gauge

interactions and working in a QCD-improved top+bottom Yukawa model, with the Lagrangian

$$\mathcal{L} = -\frac{1}{4}G^{a\mu\nu}G_{\mu\nu}^a + \bar{t}iD_t + \bar{b}iD_b + |\partial_\mu\phi|^2 - V(\phi) - g_t\bar{Q}_L\phi^ct_R - g_b\bar{Q}_L\phi b_R \quad (12)$$

$$\begin{aligned} V(\phi) &= -\mu^2|\phi|^2 + \frac{\lambda}{2}|\phi|^4 \\ &= -\frac{M_H^2}{8}v^2 + \frac{M_H^2}{2}H^2 + \frac{M_H^2}{v}\left[\frac{H^3}{2} + \frac{H}{2}(G^0)^2 + HG^+G^-\right] \\ &\quad + \frac{M_H^2}{2v^2}\left[\frac{H^4}{4} + \frac{H^2}{2}(G^0)^2 + H^2G^+G^- + (G^+G^-)^2 + (G^0)^2G^+G^- + \frac{(G^0)^4}{4}\right]. \end{aligned} \quad (13)$$

Here, we define the Yukawa couplings as $g_{t/b} = \sqrt{2}m_{t/b}/v$, and the covariant derivative D_μ with respect to QCD. The left-handed quark isospin doublet is given by

$$Q_L = \begin{pmatrix} t \\ b \end{pmatrix}_L, \quad (14)$$

with t_R denoting the right-handed top-quark field. The scalar Higgs isodoublet is defined as¹

$$\phi = \begin{pmatrix} G^+ \\ \frac{v + H + iG^0}{\sqrt{2}} \end{pmatrix}, \quad (15)$$

where H is the physical Higgs field and G^\pm, G^0 are the charged and neutral Goldstone bosons, respectively. The Higgs potential is denoted by $V(\phi)$. The vacuum expectation value is given by $v^2 = 2\mu^2/\lambda$ and the Higgs mass by $M_H^2 = \lambda v^2$ in terms of the two initial parameters μ^2, λ of the Higgs potential. Within the gaugeless limit, the Goldstones are massless,

$$M_{G^0} = M_{G^\pm} = 0. \quad (16)$$

The neutral and charged Goldstones couple to the top quark with the top Yukawa coupling, too, and thus need to be taken into account to define the full top-Yukawa induced corrections consistently².

3.1.1 Two-loop triangle diagrams

The two-loop diagrams contributing to the top-Yukawa induced component of Δ_Δ can be split into one-loop times one-loop diagrams, and triangle and box diagrams which generate the single- and double-Higgs couplings to gluons. The two-loop box diagrams will be discussed in the next paragraph. The one-loop times one-loop diagrams have been discussed in Ref. [26] and lead

¹ $\phi^c = i\sigma^2\phi^*$ denotes the charge-conjugated Higgs doublet.

²In unitary gauge of the full electroweak sector, the top-Yukawa coupling of the would-be Goldstones is hidden in the contributions of the longitudinal W, Z components and needs to be extracted by suitable expansions in the large top-mass limit for a complete top-Yukawa induced contribution.

to the correction Δ_{HHH} , while the two-loop triangle diagrams, depicted in Fig. 2, result in the correction term δ_1 ,

$$\Delta_\Delta = \Delta_{HHH} + \delta_1. \quad (17)$$

The analytical result of Δ_{HHH} can be found in Ref. [26].

For the two-loop triangle diagrams we have used the same method as described in Ref. [16], i.e. we introduced suitable Feynman parametrizations of each diagram individually, performed end-point subtractions to separate the divergences, and applied integrations by parts of the integrands to reduce the power of the denominators, which stabilize the numerical integrations above the individual virtual thresholds. In all diagrams, we encounter virtual $t\bar{t}$ and $t\bar{t}H$ thresholds. For charged Goldstone exchanges, there is an additional virtual $b\bar{b}$ threshold which induces the largest instabilities of the three. To regularize the virtual thresholds we have introduced small imaginary parts of the propagator masses,

$$m_{t/b}^2 \rightarrow m_{t/b}^2(1 - i\bar{\epsilon}), \quad M_H^2 \rightarrow M_H^2(1 - i\bar{\epsilon}) \quad (18)$$

and performed Richardson extrapolations to obtain the limit $\bar{\epsilon} \rightarrow 0$.

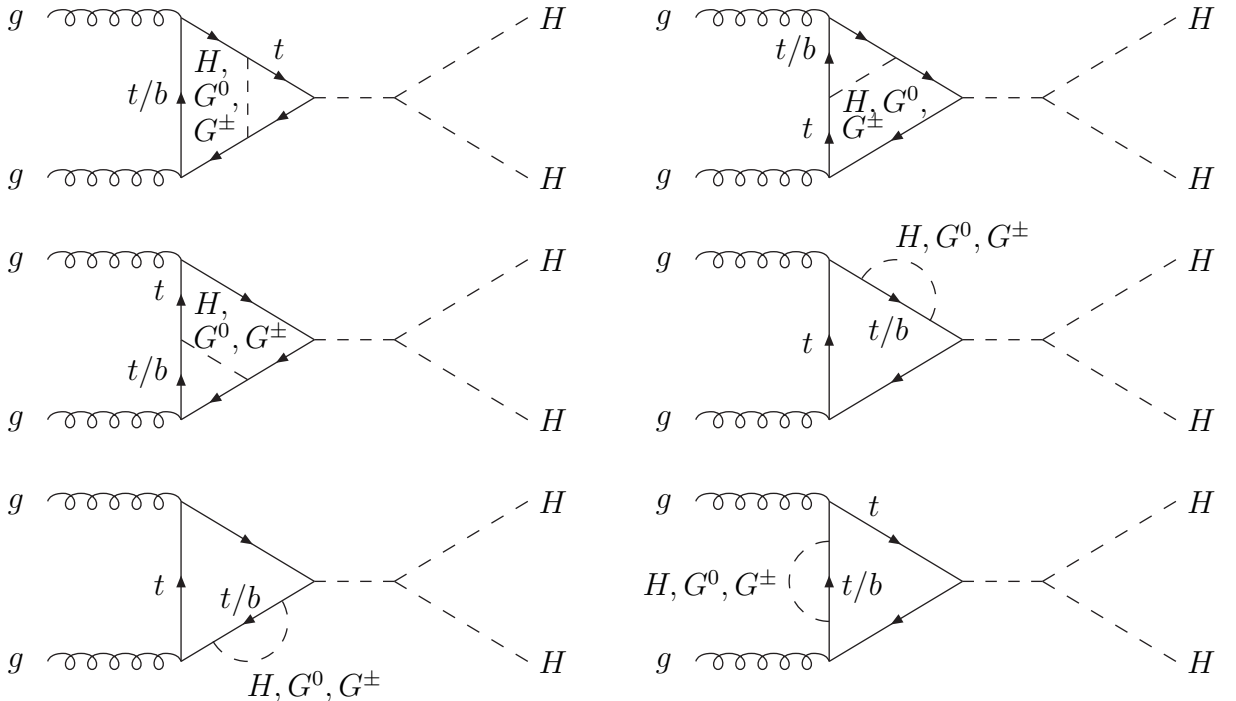


Figure 2: Two-loop triangle diagrams of the top-Yukawa-induced electroweak corrections to Higgs-boson pair production involving Higgs H and Goldstone G^0, G^\pm exchanges. The bottom propagators only contribute to the diagrams with charged Goldstone exchange.

The counterterm $\delta_{1,CT}$ for the two-loop triangle diagrams consists of the counterterms for the on-shell Higgs wave function³, the vacuum expectation value⁴ and the top mass that is

³Half of this counterterm is already contained in the correction Δ_{HHH} .

⁴This counterterm is determined from the muon decay in the G_F scheme.

renormalized on-shell ($x_t = G_F m_t^2 / (8\sqrt{2}\pi^2)$),

$$\begin{aligned}
\delta_{1,CT} &= \frac{\delta Z_H}{2} - \frac{\delta v}{v} - 2\delta m_t \frac{1}{F_\Delta} \frac{\partial F_\Delta}{\partial m_t} \\
\delta Z_H = \Sigma'_H(Q^2) &= 6x_t \{ (4m_t^2 - Q^2) B'_0(Q^2; m_t, m_t) - B_0(Q^2; m_t, m_t) \} \\
\frac{\delta v}{v} = \frac{1}{2} \frac{\Sigma_W(0)}{M_W^2} &= \frac{T_1}{v M_H^2} + x_t \{ B_0(0; m_t, m_b) + 2B_0(0; m_t, m_t) + m_t^2 B'_0(0; m_t, m_b) \} \\
\frac{\delta m_t}{m_t} = \frac{\Sigma(m_t)}{m_t} &= \frac{T_1}{v M_H^2} - x_t \left\{ \left(2 - \frac{M_H^2}{2m_t^2} \right) B_0(p; m_t, M_H) + \frac{m_t^2 + m_b^2}{2m_t^2} B_0(p; m_b, 0) \right. \\
&\quad \left. + \frac{A_0(M_H) - 2A_0(m_t) - A_0(m_b)}{2m_t^2} \Big|_{p^2=m_t^2} \right\} \tag{19}
\end{aligned}$$

where we keep the bottom mass m_b in the arguments of the scalar integrals and the tadpole contribution is given by

$$\frac{T_1}{v} = -12x_t A_0(m_t). \tag{20}$$

The functions $\Sigma_{W,t}$ are the self-energies of the W boson and the top quark, respectively, while Σ'_H denotes the derivative of the Higgs self-energy with respect to Q^2 . We have checked explicitly that the tadpole contributions cancel against the two-loop tadpole diagrams by introducing tadpole insertions for all of the virtual LO top-quark propagators (see Fig. 3). The scalar integrals A_0, B_0, C_0 are the usual 't Hooft–Veltman one-loop integrals [31] and

$$B'_0(q^2; m_1, m_2) = \frac{\partial}{\partial q^2} B_0(q^2; m_1, m_2). \tag{21}$$

The correction factor δ_1 of Eq. (17) summarizes the combined result of the two-loop triangle diagrams and counterterms. Until now, δ_1 has only been calculated in the HTL ($\delta_1 \rightarrow x_t/2$). As a cross-check, we artificially increased the top mass to 3 TeV in our computations and confirmed that δ_1 coincides with this limit within numerical errors.

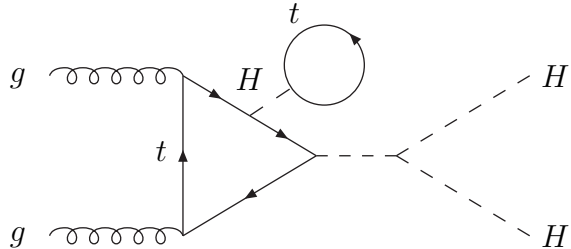


Figure 3: Example of a two-loop tadpole diagram of the top-Yukawa induced electroweak corrections to Higgs-boson pair production involving Higgs exchange. Goldstone exchange does not contribute to the tadpoles.

The final result of the correction factor $\delta_1 \equiv C_1 x_t$ is shown in Fig. 4 as a function of the invariant Higgs-pair mass M_{HH} . Note that $Q^2 = M_{HH}^2$ is the squared momentum that flows

through the s -channel Higgs propagator. Multiplying the shown factor C_1 with $x_t \sim 0.3\%$, the total corrections stay below the per-cent level.

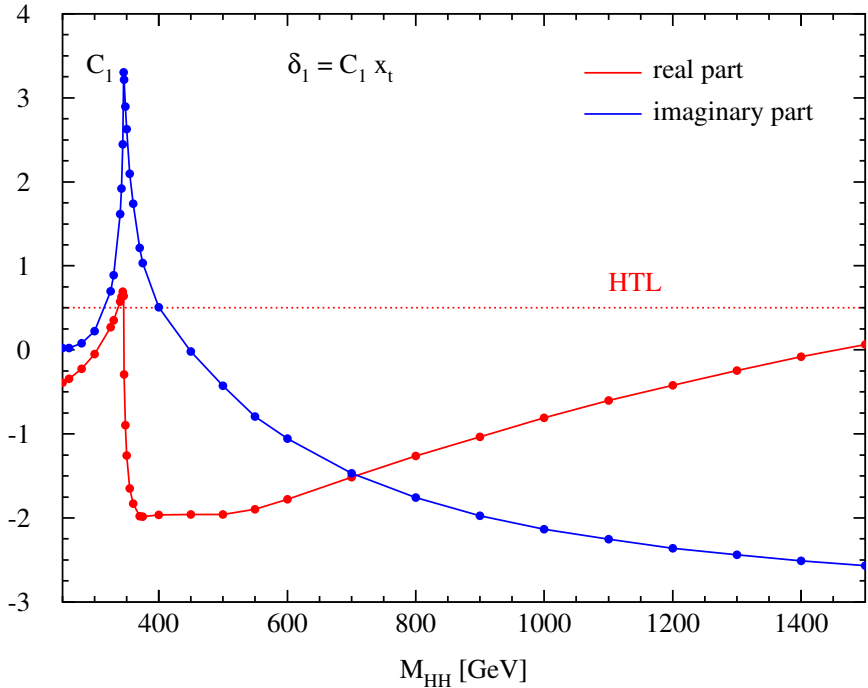


Figure 4: The relative top-Yukawa-induced electroweak correction factor δ_1 as a function of the invariant Higgs-pair mass M_{HH} with the top-Yukawa factor x_t stripped off. The dots along the curves represent the numerical numbers we generated. The dotted curve shows the HTL of the full result, $C_1 \rightarrow 1/2$ for large values of m_t .

3.1.2 Two-loop box diagrams

Sample two-loop diagrams describing the genuine box contributions to the top-Yukawa induced electroweak corrections (Δ_\square, Δ_G) are shown in Fig. 5. To obtain the numerical integrals, we apply the projectors of Eq. (10) on the two form factors, Feynman parametrization and endpoint subtractions on every diagram. To stabilize the numerical diagrams above the virtual thresholds, we performed integration-by-parts and the analytical continuation of the propagator masses according to Eq. (18). Finally, Richardson extrapolations are used to reach the limit $\bar{\epsilon} \rightarrow 0$. In this context, we have modified the extrapolation polynomials used in Refs. [15, 16] in the vicinity of the $t\bar{t}$ threshold, since it was observed in [32] that the $\bar{\epsilon}$ dependence close to the threshold is not polynomial in $\bar{\epsilon}$ but in $\sqrt{\bar{\epsilon}}$. This behavior can be accommodated by modifying

the original polynomials displayed in Eq. (3.33) of Ref. [16]⁵ to

$$\begin{aligned}
R_1(\bar{\epsilon}) &= \frac{\sqrt{2}I(\bar{\epsilon}) - I(2\bar{\epsilon})}{\sqrt{2} - 1} \\
R_2(\bar{\epsilon}) &= \frac{2\sqrt{2}I(\bar{\epsilon}) - (2 + \sqrt{2})I(2\bar{\epsilon}) + I(4\bar{\epsilon})}{\sqrt{2} - 1} \\
R_3(\bar{\epsilon}) &= \frac{-8I(\bar{\epsilon}) + 2(2 + 3\sqrt{2})I(2\bar{\epsilon}) - (2 + 3\sqrt{2})I(4\bar{\epsilon}) + I(8\bar{\epsilon})}{3\sqrt{2} - 5} \\
R_4(\bar{\epsilon}) &= \frac{-32I(\bar{\epsilon}) + 24(1 + \sqrt{2})I(2\bar{\epsilon}) - 6(2 + 3\sqrt{2})I(4\bar{\epsilon}) + 3(2 + \sqrt{2})I(8\bar{\epsilon}) - I(16\bar{\epsilon})}{3(3\sqrt{2} - 5)} \quad (22)
\end{aligned}$$

and so forth. We used these polynomials in the region of ± 1 GeV around the $t\bar{t}$ threshold for the Richardson extrapolation.

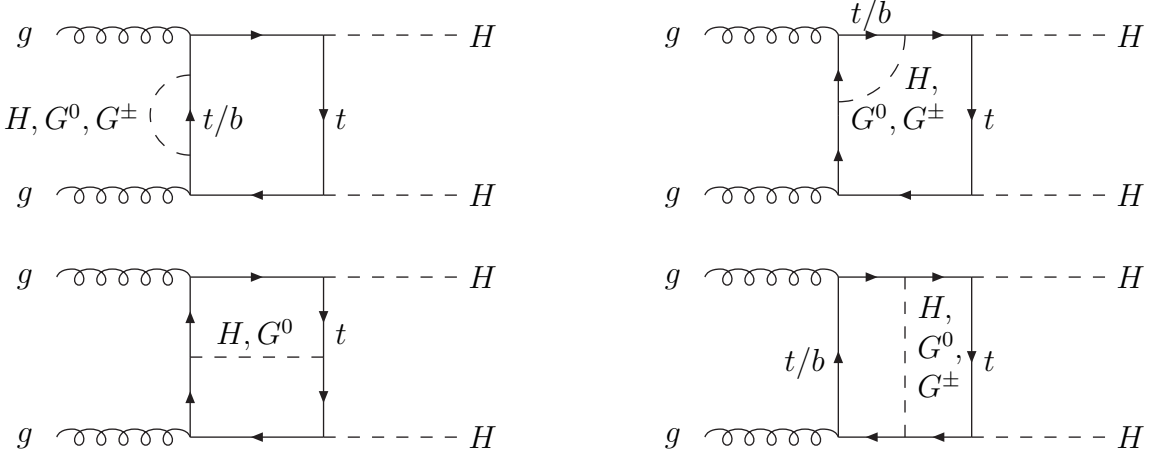


Figure 5: Sample two-loop box diagrams of the top-Yukawa-induced electroweak corrections to Higgs-boson pair production involving Higgs H and Goldstone G^0, G^\pm exchanges. The bottom propagators only contribute to the diagrams with charged Goldstone exchange.

The on-shell Higgs wave function, vacuum expectation value and on-shell top mass counterterms appear in the counterterms of the two-loop box diagrams. They are given by

$$\begin{aligned}
\Delta_{\square,CT} &= \delta Z_H - 2\frac{\delta v}{v} - 2\delta m_t \frac{1}{F_\square} \frac{\partial F_\square}{\partial m_t} \\
\Delta_{G,CT} &= \delta Z_H - 2\frac{\delta v}{v} - 2\delta m_t \frac{1}{G_\square} \frac{\partial G_\square}{\partial m_t}
\end{aligned} \quad (23)$$

⁵With the polynomial dependence $I(\bar{\epsilon}) = \sum_i c_i \bar{\epsilon}^{i/2}$ the Richardson polynomials behave as $R_i(\bar{\epsilon}) = I(0) + \mathcal{O}(\bar{\epsilon}^{(i+1)/2})$.

for the two form factors F_{\square} and G_{\square} , respectively. The final results are summarized by the finite correction factors $\Delta_{\square}, \Delta_G$ of Eq. (6). It is known that in the HTL, $\Delta_{\square} \rightarrow 4x_t$ [26], and we have checked numerically that this limit is reproduced by our numerical calculation within numerical errors by artificially increasing the size of the virtual top mass to 3 TeV.

3.2 Light-Quark-induced corrections

The second class of electroweak corrections we have calculated is the light-quark-loop induced corrections. We take into account closed loops of all light-quark flavors up to the bottom quark in diagrams involving Z bosons, and up to the charm quark in diagrams involving W bosons, in order to avoid top-quark contributions. Also, we do *not* work in the gaugeless limit in this case. For single-Higgs production, these types of corrections were the dominant part of the full NLO electroweak corrections [33, 34]. The corresponding Higgs-pair diagrams are split into three different classes: the triangle diagrams with an s -channel Higgs propagator, the triangle-like diagrams with a four-point $WWHH$ and $ZZHH$ interaction and the genuine double-box contributions, see Fig. 6.

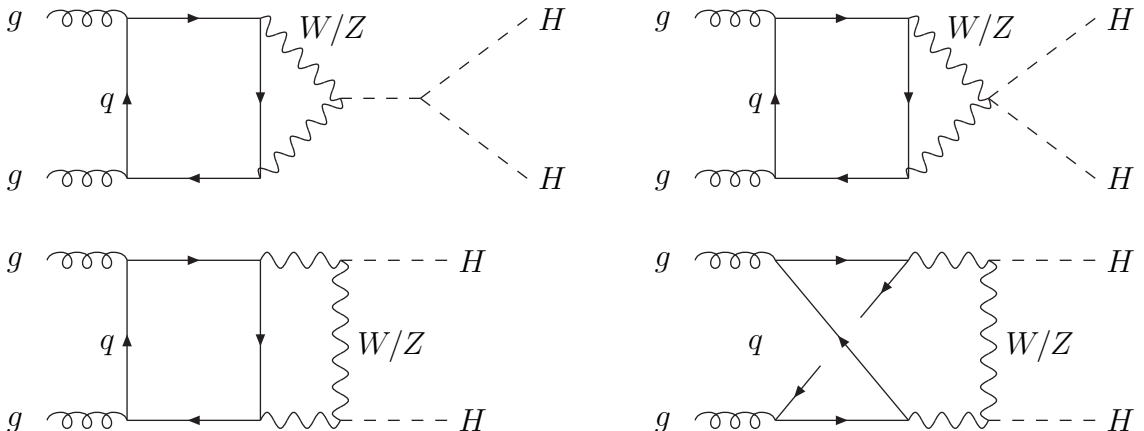


Figure 6: *Sample two-loop box diagrams of the light-quark-induced electroweak corrections to Higgs-boson pair production. Shown are diagrams of the three classes – triangle diagrams, four-point diagrams and genuine planar/non-planar double boxes.*

We have applied the same method as for the top-Yukawa induced diagrams for these corrections, i.e. suitable Feynman parametrizations of the individual diagrams after projecting onto the two form factors, end-point subtractions to separate the divergencies and integration-by-parts to stabilize the virtual thresholds, where we introduced complex propagator masses (including the W and Z boson masses, $M_{W/Z}^2 \rightarrow M_{W/Z}^2(1 - i\bar{\epsilon})$) as in Eq. (18). We have explicitly checked that there are no infrared or collinear divergences in the individual diagrams, so end-point subtractions alone are sufficient to isolate the divergences. The UV poles cancel between the planar and non-planar box diagrams, as well as for the triangle and four-point diagrams individually. As a quantitative cross-check, we implemented the corresponding results of

the single Higgs case [33] and compared them against our results for the triangle diagrams and the four-point diagrams and found full agreement with our numerical implementation. For the sake of accuracy and stability, we computed the numerical results with these implementations. For the genuine double-box diagrams, the dependence on the imaginary parameter $\bar{\epsilon}$ is mild; therefore, we computed the results with the value $\bar{\epsilon} = 0.05$, as this has been found to be in the plateau of the narrow-width limit $\bar{\epsilon} \rightarrow 0$ within integration errors. The results of the triangle diagrams can be accommodated by the same correction factor δ_1 as in the top-Yukawa induced part, see Eq. (17). The emerging contribution $\delta_{1,lq}$ is shown in Fig. 7 and amounts to less than a per-cent in total.

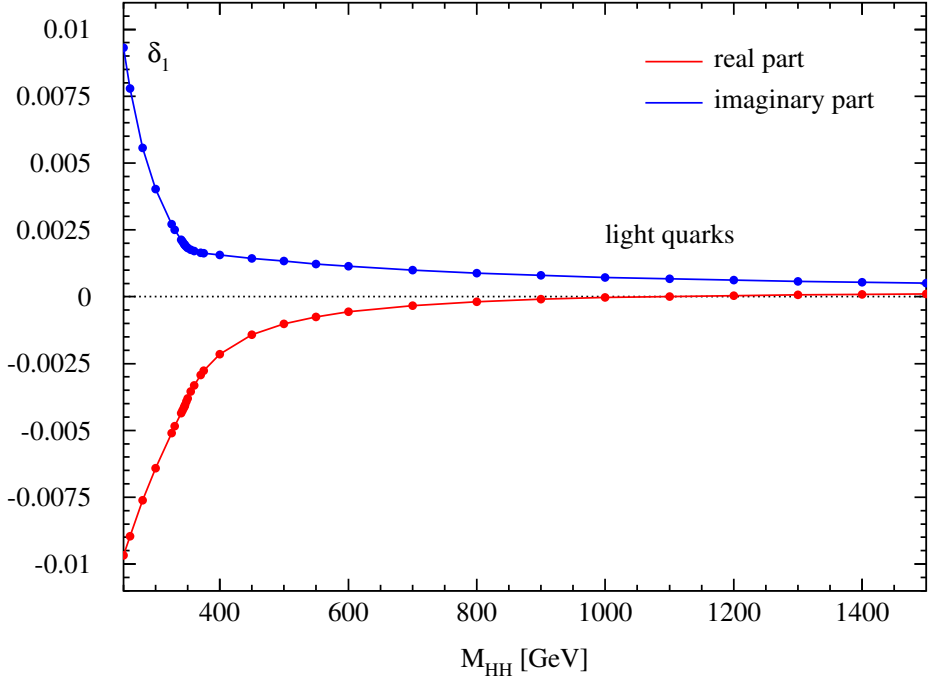


Figure 7: The relative light-quark-induced electroweak correction factor δ_1 as a function of the invariant Higgs-pair mass M_{HH} . The dots along the curves represent the numerical numbers we have generated. Their error bars are negligible and thus not shown.

4 Results

Now, we are in the position to present the relative top-Yukawa and light-quark induced electroweak corrections to Higgs-pair production via gluon fusion.

Before we move to the total electroweak corrections δ of Eq. (7), we discuss the individual contributions of the top-Yukawa and light-quark induced components,

$$\begin{aligned} \delta &= \delta_{top-Yukawa} + \delta_{light-quarks} \\ \delta_{top-Yukawa} &= \delta_{triangle} + \delta_{HHH} + \delta_{box} \end{aligned} \quad (24)$$

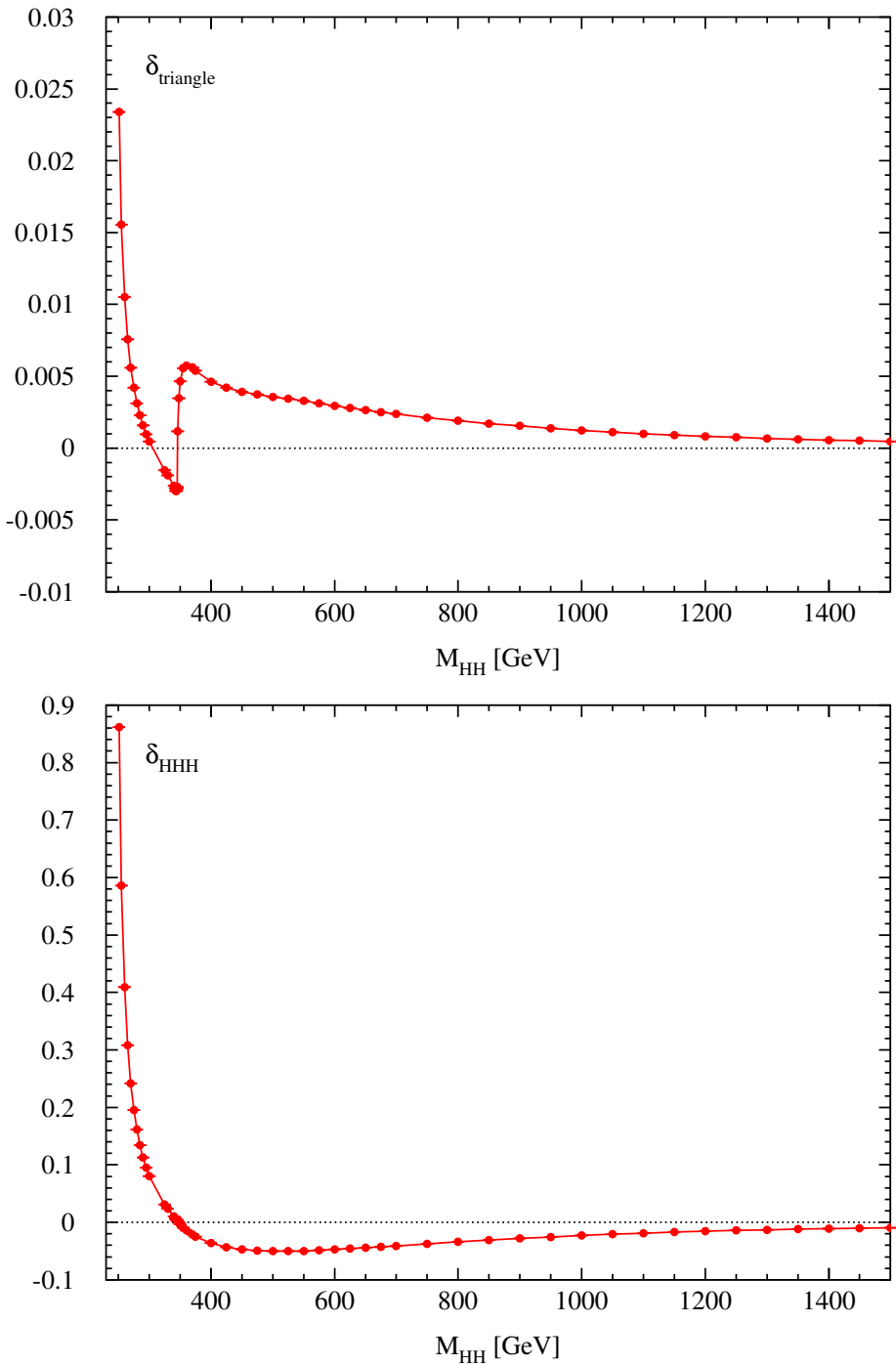


Figure 8: The relative two-loop triangle (upper plot) and one-loop times one-loop (lower plot) contributions to the electroweak corrections of the Higgs-pair production cross section as a function of the invariant Higgs-pair mass M_{HH} . The dots along the curves represent the numerical numbers we have generated.

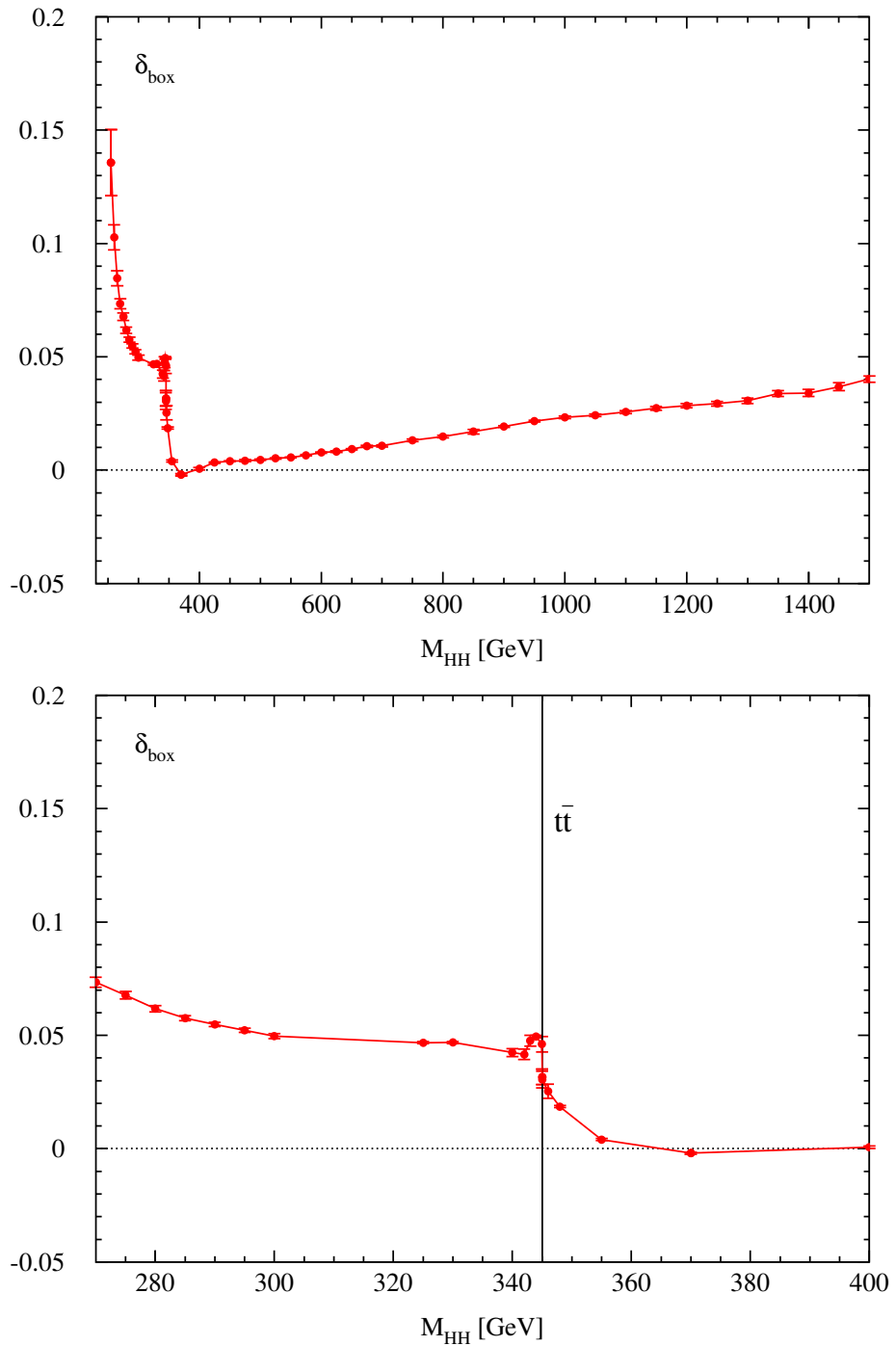


Figure 9: *The relative two-loop box contribution to the electroweak corrections of the Higgs-pair production cross section as a function of the invariant Higgs-pair mass M_{HH} . The lower plot shows the magnified region around the $t\bar{t}$ threshold. The dots along the curves represent the numerical numbers we have generated and their error bars.*

In Fig. 8, the individual contributions of the two-loop triangle and one-loop times one-loop diagrams are shown. The size of the triangle-diagram part ranks at the per-cent level in most of the invariant Higgs-pair mass range, apart from the region close to the production threshold $M_{HH} \gtrsim 2M_H$. In this region, the corrections are larger, since they are lifting the strong cancelation of the triangle and box diagrams at LO. On the other hand, the contribution δ_{HHH} emerging from the one-loop times one-loop diagrams, Δ_{HHH} of Eq. (17), is significantly larger, at the -5% level for larger invariant Higgs-pair masses M_{HH} as displayed in the lower part of Fig. 8. These corrections provide a sizable correction close to the production threshold, which is in line with the results of Ref. [26]. The contribution of the two-loop box diagrams, as depicted in Fig. 9, is at the $5\text{--}10\%$ level. The electroweak corrections are dominated by the contributions of form factor F_1 of Eq. (9), while form factor F_2 is only relevant for larger values of M_{HH} . To properly describe the $t\bar{t}$ threshold behavior, a deeper analysis on the convergences of the Richardson polynomials has been performed. In contrast to the other regions, the amplitudes are strongly dependent on $\bar{\epsilon}$. Thus, to ensure the narrow-width limit, the Richardson polynomial needs a minimal regulator $\bar{\epsilon} \sim 10^{-2}$. As the result, the virtual $t\bar{t}$ threshold appears as a shoulder in the invariant mass distribution with a maximum-minimum behaviour around the $t\bar{t}$ threshold. This is shown in detail in the lower plot of Fig. 9 and is in line with the \mathcal{P} -wave property of the threshold at LO that prevents a kink-like structure at NLO. Summing up all ingredients for the total top-Yukawa induced corrections, we arrive at the total relative corrections shown in Fig. 10. The total corrections amount to about $\pm 5\%$ in the large- M_{HH} regime, while they are larger close to the production threshold.

As an additional contribution to the electroweak corrections, the total result of the light-quark induced electroweak corrections, denoted by $\delta_{\text{light-quarks}}$, is shown in Fig. 11. We implemented a Richardson extrapolation for two values of the imaginary regulator, $\bar{\epsilon} = 0.1$ and 0.05 , which proved sufficient to reach the narrow-width limit across the full range of M_{HH} . These corrections are dominated by the form factor F_1 of Eq. (9), while the form factor F_2 becomes relevant only for larger values of the invariant Higgs-pair mass M_{HH} . The light-quark contributions are small for large invariant Higgs-pair masses M_{HH} and are relevant only close to the production threshold, where they are negative.

Using a suitable interpolation of our results implemented in the code `Hpair` [35] we arrive at the individual corrections to the total hadronic cross section that amount to -1.9% for the top-Yukawa induced part and -1.5% for the light-quark induced corrections. In total, our corrections as part of the full electroweak corrections reduce the total cross section by 3.4% .

5 Conclusions

In this work, we calculated the top-Yukawa and light-quark induced electroweak corrections to Higgs-pair production via gluon fusion, $gg \rightarrow HH$. We applied the same numerical methods as in the case of the QCD corrections at NLO [15, 16], i.e. projection on the two physical form factors of the spin-0 and 2 contributions, Feynman parametrization of all two-loop diagrams individually, end-point subtractions to separate the ultraviolet divergences and integration-by-parts to stabilize the numerical integrals across the virtual thresholds. Above the virtual

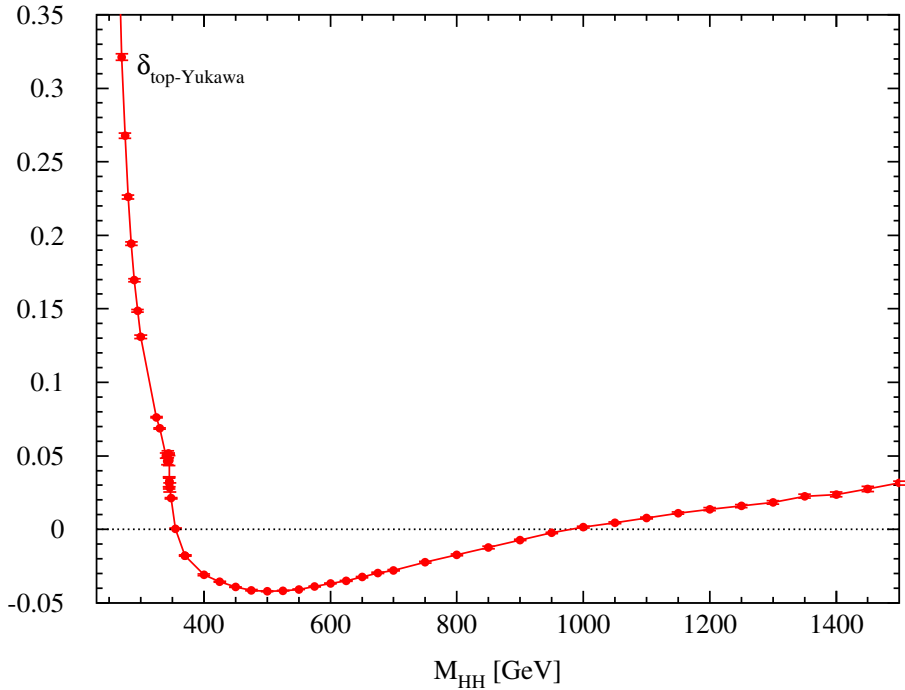


Figure 10: *The relative total two-loop top-Yukawa induced contribution to the electroweak corrections of the Higgs-pair production cross section as a function of the invariant Higgs-pair mass M_{HH} . The dots along the curves represent the numerical numbers we have generated and their error bars.*

thresholds, we introduced complex propagator masses with a small imaginary part and used Richardson extrapolations to arrive at the narrow-width limit. The total top-Yukawa induced corrections amount to the level of 5–10% for moderate and large values of the invariant Higgs-pair mass M_{HH} , while they are larger close to the production threshold $M_{HH} \gtrsim 2M_H$ due to the strong destructive interference of the LO matrix element. The top-Yukawa induced corrections develop a shoulder at the virtual $t\bar{t}$ threshold that is in line with the \mathcal{P} -wave nature of this threshold at LO. For larger values of M_{HH} , we observe a finite slope in the relative corrections that modify the differential cross section by a few per-cent up to the 5%-level. On the other hand, the light-quark induced corrections are tiny in the large M_{HH} range and only contribute significantly close to the production threshold, again, due to strong suppression of the LO matrix element. The individual corrections to the total hadronic cross section amount to -1.9% for the top-Yukawa induced part and -1.5% for the light-quark induced corrections. This work presents the first steps towards the calculation of the full electroweak corrections.

Acknowledgments

The authors are indebted to M. Bonetti, C. Borschensky, G. Heinrich, S. Jones, M. Kerner, P. Rendler, and A. Vestner for useful discussions. We would like to thank M. Bonetti and P. Rendler for comparing explicit numbers of the light-quark induced corrections. The work of A.B. and F.C. is supported by the Generalitat Valenciana, the Spanish government, and

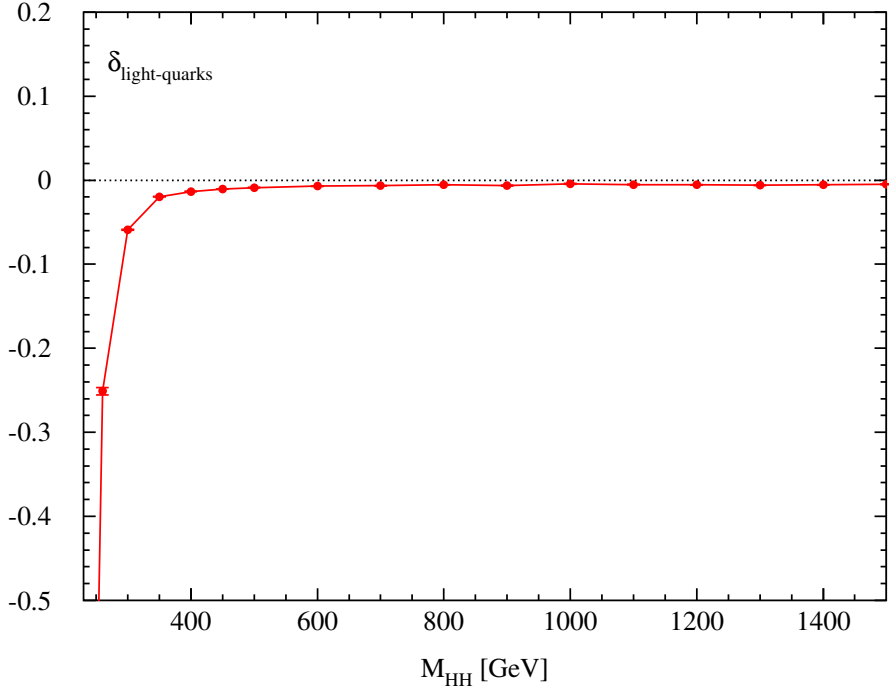


Figure 11: *The relative light-quark-induced contribution to the electroweak corrections of the Higgs-pair production cross section as a function of the invariant Higgs-pair mass M_{HH} . The dots along the curves represent the numerical numbers we have generated and their error bars.*

ERDF funds from the European Commission “NextGenerationEU/PRTR” (CNS2022-136165, PID2023-151418NB-I00, MCIN/AEI/10.13039/501100011033/). The research of S.C. and M.M. is supported by the Deutsche Forschungsgemeinschaft (DFG, German Research Foundation) under grant 396021762–TRR 257. The work of J.C. is supported by the Swiss National Science Foundation (SNSF). J.R. acknowledges support from INFN. We acknowledge support by the state of Baden-Württemberg through bwHPC and the German Research Foundation (DFG) through grant no INST 39/963-1 FUGG (bwForCluster NEMO).

References

- [1] G. Aad *et al.* [ATLAS Collaboration], Phys. Lett. **B716** (2012) 1; S. Chatrchyan *et al.* [CMS Collaboration], Phys. Lett. **B716** (2012) 30.
- [2] G. Aad *et al.* [ATLAS and CMS Collaborations], JHEP **1608** (2016) 045; G. Aad *et al.* [ATLAS Collaboration], ATLAS-CONF-2019-005; A.M. Sirunyan *et al.* [CMS Collaboration], JHEP **01** (2021) 148.
- [3] G. Aad *et al.* [ATLAS], Phys. Lett. B **809** (2020), 135754 and arXiv:2507.12598 [hep-ex]; A. Tumasyan *et al.* [CMS], JHEP **05** (2023), 233.
- [4] A. Djouadi, W. Kilian, M. Mühlleitner and P.M. Zerwas, Eur. Phys. J. **C10** (1999), 45.

- [5] P. W. Higgs, Phys. Lett. **12** (1964) 132, Phys. Rev. Lett. **13** (1964) 508 and Phys. Rev. **145** (1966) 1156; F. Englert and R. Brout, Phys. Rev. Lett. **13** (1964) 321; G. S. Guralnik, C. R. Hagen and T. W. Kibble, Phys. Rev. Lett. **13** (1964) 585; T. W. B. Kibble, Phys. Rev. **155** (1967) 1554.
- [6] C. H. Llewellyn Smith, Phys. Lett. **46B** (1973) 233; J. M. Cornwall, D. N. Levin and G. Tiktopoulos, Phys. Rev. D **10** (1974) 1145 Erratum: [Phys. Rev. D **11** (1975) 972]; B. W. Lee, C. Quigg and H. B. Thacker, Phys. Rev. Lett. **38** (1977) 883 and Phys. Rev. D **16** (1977) 1519.
- [7] G. 't Hooft, Nucl. Phys. B **35** (1971) 167; G. 't Hooft and M. J. G. Veltman, Nucl. Phys. B **44** (1972) 189.
- [8] M. Spira, Fortsch. Phys. **46** (1998) 203 and Prog. Part. Nucl. Phys. **95** (2017) 98; A. Djouadi, Phys. Rept. **457** (2008), 1-216.
- [9] J. Baglio, A. Djouadi, R. Gröber, M. M. Mühlleitner, J. Quevillon and M. Spira, JHEP **1304** (2013) 151; B. Di Micco, M. Gouzevitch, J. Mazzitelli, C. Vernieri, J. Alison, K. Androsov, J. Baglio, E. Bagnaschi, S. Banerjee and P. Basler, *et al.*, Rev. Phys. **5** (2020) 100045.
- [10] E. W. N. Glover and J. J. van der Bij, Nucl. Phys. **B309** (1988) 282; T. Plehn, M. Spira and P. M. Zerwas, Nucl. Phys. **B479** (1996) 46, Erratum: [Nucl. Phys. **B531** (1998) 655].
- [11] S. Dawson, S. Dittmaier and M. Spira, Phys. Rev. **D58** (1998) 115012.
- [12] D. de Florian and J. Mazzitelli, Phys. Lett. B **724** (2013) 306 and Phys. Rev. Lett. **111** (2013) 201801; J. Grigo, K. Melnikov and M. Steinhauser, Nucl. Phys. B **888** (2014) 17.
- [13] L. B. Chen, H. T. Li, H. S. Shao and J. Wang, Phys. Lett. **B803** (2020) 135292 and JHEP **2003** (2020) 072.
- [14] S. Borowka, N. Greiner, G. Heinrich, S. P. Jones, M. Kerner, J. Schlenk, U. Schubert and T. Zirke, Phys. Rev. Lett. **117** (2016) no.1, 012001 Erratum: [Phys. Rev. Lett. **117** (2016) no.7, 079901]; S. Borowka, N. Greiner, G. Heinrich, S. P. Jones, M. Kerner, J. Schlenk and T. Zirke, JHEP **1610** (2016) 107.
- [15] J. Baglio, F. Campanario, S. Glaus, M. Mühlleitner, M. Spira and J. Streicher, Eur. Phys. J. **C79** (2019) no.6, 459; J. Baglio, F. Campanario, S. Glaus, M. Mühlleitner, J. Ronca and M. Spira, Phys. Rev. **D103** (2021) no.5, 056002.
- [16] J. Baglio, F. Campanario, S. Glaus, M. Mühlleitner, J. Ronca, M. Spira and J. Streicher, JHEP **04** (2020), 181.
- [17] J. Grigo, K. Melnikov and M. Steinhauser, Nucl. Phys. B **888** (2014), 17-29; J. Grigo, J. Hoff and M. Steinhauser, Nucl. Phys. B **900** (2015), 412-430; R. Gröber, A. Maier and T. Rauh, JHEP **03** (2018), 020; R. Bonciani, G. Degrassi, P. P. Giardino and R. Gröber,

Phys. Rev. Lett. **121** (2018) no.16, 162003; J. Davies, G. Mishima, M. Steinhauser and D. Wellmann, JHEP **01** (2019), 176; J. Davies, G. Heinrich, S. P. Jones, M. Kerner, G. Mishima, M. Steinhauser and D. Wellmann, JHEP **11** (2019), 024; L. Bellafronte, G. Degrassi, P. P. Giardino, R. Gröber and M. Vitti, JHEP **07** (2022), 069.

[18] E. Bagnaschi, G. Degrassi and R. Gröber, Eur. Phys. J. C **83** (2023) no.11, 1054.

[19] D. de Florian and J. Mazzitelli, Phys. Lett. B **724** (2013) 306 and Phys. Rev. Lett. **111** (2013) 201801; J. Grigo et al., Nucl. Phys. **B888** (2014) 17; M. Grazzini, G. Heinrich, S. Jones, S. Kallweit, M. Kerner, J. M. Lindert and J. Mazzitelli, JHEP **1805** (2018) 059.

[20] D. Y. Shao, C. S. Li, H. T. Li and J. Wang, JHEP **07** (2013), 169; D. de Florian and J. Mazzitelli, JHEP **09** (2015), 053 and JHEP **08** (2018), 156; A. H. Ajjath and H. S. Shao, JHEP **02** (2023), 067.

[21] G. Heinrich, S. P. Jones, M. Kerner, G. Luisoni and E. Vryonidou, JHEP **08** (2017), 088; S. Jones and S. Kuttimalai, JHEP **02** (2018), 176.

[22] S. Alioli, G. Marinelli and D. Napoletano, arXiv:2507.08558 [hep-ph].

[23] J. Davies, K. Schönwald and M. Steinhauser, Phys. Lett. B **845** (2023), 138146 and [arXiv:2503.17449 [hep-ph]]; J. Davies, K. Schönwald, M. Steinhauser and M. Vitti, JHEP **08** (2024), 096.

[24] S. Jaskiewicz, S. Jones, R. Szafron and Y. Ulrich, [arXiv:2501.00587 [hep-ph]].

[25] J. R. Espinosa and R. J. Zhang, Nucl. Phys. B **586** (2000), 3-38; A. Brignole, G. Degrassi, P. Slavich and F. Zwirner, Nucl. Phys. B **631** (2002), 195-218.

[26] M. Mühlleitner, J. Schlenk and M. Spira, JHEP **10** (2022), 185.

[27] H. Y. Bi, L. H. Huang, R. J. Huang, Y. Q. Ma and H. M. Yu, Phys. Rev. Lett. **132** (2024) no.23, 231802.

[28] G. Heinrich, S. Jones, M. Kerner, T. Stone and A. Vestner, JHEP **11** (2024), 040.

[29] J. Davies, G. Mishima, K. Schönwald, M. Steinhauser and H. Zhang, JHEP **08** (2022), 259, JHEP **10** (2023), 033 and JHEP **04** (2025), 193.

[30] M. Bonetti, P. Rendler and W. J. Torres Bobadilla, JHEP **07** (2025), 024.

[31] G. 't Hooft and M. J. G. Veltman, Nucl. Phys. B **153** (1979), 365-401.

[32] E. Bagnaschi, L. Fritz, S. Liebler, M. Mühlleitner, T. T. D. Nguyen and M. Spira, JHEP **03** (2023), 124; L. Fritz, PhD thesis, University of Zurich, 2023.

[33] U. Aglietti, R. Bonciani, G. Degrassi and A. Vicini, Phys. Lett. B **595** (2004) 432 and hep-ph/0610033; G. Degrassi and F. Maltoni, Phys. Lett. B **600** (2004) 255. R. Bonciani, G. Degrassi and A. Vicini, Comput. Phys. Commun. **182** (2011), 1253-1264.

- [34] S. Actis, G. Passarino, C. Sturm and S. Uccirati, Phys. Lett. B **670** (2008) 12; S. Actis, G. Passarino, C. Sturm and S. Uccirati, Nucl. Phys. B **811** (2009) 182.
- [35] <https://gitea.psi.ch/ltpth/HPAIR>